THE ASTROPHYSICAL JOURNAL, 405:720–726, 1993 March 10

PARTICLE TRANSPORT AND THE λ BOOTIS PHENOMENON. I. THE DIFFUSION/MASS-LOSS MODEL REVISITED

P. CHARBONNEAU
High Altitude Observatory, National Center for Atmospheric Research,[1] P.O. Box 3000, Boulder, CO 80307-3000
Received 1992 August 13; accepted 1992 September 15

ABSTRACT

Recent observational work has cast doubt on the validity of the diffusion-based model originally developed to account for the peculiar characteristics of the λ Bootis stars. Among some of the difficulties facing the model, the potential effects of rotation stand most prominently. The original diffusion model neglects all forms of rotationally induced mixing, be it in the form of turbulence or large-scale meridional circulation. It was already realized then that this may well be a critical omission, as meridional circulation proved to play an important role in the evolution of chemical abundances in other types of chemically peculiar stars.

In this paper, results of two-dimensional linear time-dependent particle transport calculations in a λ Bootis star are presented for two representative elements, titanium and calcium. These demonstrate unambiguously that the inclusion of meridional circulation in the original diffusion/mass-loss model of λ Bootis stars has profound consequences on the abundance evolution. More specifically, circulation prevents the appearance, at any epoch of main-sequence evolution, of the underabundance patterns characteristic of λ Bootis stars. This indicates that the diffusion/mass-loss model for these objects must be either abandoned or significantly modified. Caveats and possible alternatives are discussed, and a few observational tests are suggested.

Subject headings: diffusion — stars: abundances — stars: interiors — stars: mass-loss — stars: peculiar — stars: rotation

1. INTRODUCTION

The existence of a restricted class of chemically peculiar stars of which λ Boo is the prototype has been known for nearly half a century (see e.g., Morgan, Keenan, & Kellman 1943). Yet it is only recently that the basic characteristics of these rare objects became well-defined (the class includes 22 objects as of 1992; for a recent review see Gerbaldi & Faraggiana 1993). They are Population I main-sequence stars (Baschek & Searle 1969), found relatively close to the ZAMS in the relatively narrow spectral type interval A0–F0 (Gray 1988). They show no evidence of strong large-scale surface magnetic fields (Bohlender & Landstreet 1990). Inasmuch as one is willing to attach some weight to a $v \sin i$ distribution constructed out of 18 stars, rotationally they appear similar to chemically normal stars in the same spectral type interval, except for an apparent lack of slow ($v \sin i \lesssim 50$ km s^{-1}) rotators.

From the standpoint of chemical abundances, the λ Bootis "signature" is characterized by essentially normal C, N, O and probably S, but underabundances of all heavier metals. Traditionally, underabundances by factors of 3–5 were quoted, with somewhat larger values for Mg and Ca (e.g., Baschek & Slettebak 1988, and references therein). More recently, Venn & Lambert (1990) obtained, in their final analysis, significantly larger underabundances levels (as high as 10^2) in the three λ Bootis stars that they observed. Although star-to-star variations exist, these underabundances appear to show no systematic dependence on effective temperature and/or rotation rate.

Such abundance patterns are in stark contrast to those observed in the more common FmAm stars, another class of chemically peculiar stars found in this region of the H-R diagram (Preston 1974; Cayrel et al. 1991). FmAm stars are also Population I, nonmagnetic main-sequence stars, showing underabundance in Ca and Sc (by factors of 3–10), but large *over*abundances of most heavier metals (by factors up to 500, but more typically 10–100). The FmAm phenomenon has been explained quite successfully on the basis of chemical separation in the outer radiative envelope. The key to the appearance of the FmAm abundance signature is the disappearance, following the gravitational settling of He out of the surface layers, of the part of the outer convection zone (CZ) associated with the ionization of He (see, e.g., Michaud et al. 1983; Charbonneau & Michaud 1991, hereafter CM91). In its simplest form, the model reproduces, without arbitrary parameters, both the abundance patterns and the cutoff in the observed $v \sin i$ distribution. The quantitative reproduction of the abundance anomalies, however, requires the introduction of an additional assumption (involving an arbitrary parameter), namely, that these stars undergo mass loss at a rate of order $10^{-15}\ M_\odot$ yr^{-1}.

How can otherwise similar stars show such strikingly different abundance patterns? This initially appeared to pose a difficulty for the diffusion-based explanation for chemically peculiar stars, until Michaud & Charland (1986, hereafter MC86) showed that the λ Bootis abundance "signature" would occur naturally if these stars were also assumed to be otherwise normal A stars undergoing mass loss at a higher rate of order $10^{-13}\ M_\odot$ yr^{-1}. The abundance patterns differ from those of FmAm stars for two reasons. First, the high mass-loss rate impedes He settling enough to prevent the disappearance of the superficial helium convection zone, the sine qua non condition for the appearance of the FmAm abundance signature. Second, mass loss occurs now rapidly enough that over the main-sequence lifetime, material originally located deep in

[1] The National Center for Atmospheric Research is sponsored by the National Science Foundation.

the envelope,[2] and thus depleted in most chemical species, has time to be advected to the surface, leading to the appearance of surface underabundances.

As it stood in 1986, the diffusion/mass-loss model for λ Bootis stars faced two apparent difficulties, both already recognized by MC86: First, for most elements underabundances at the required level materialized only after 10^9 yr or so. This age being of the order of or slightly inferior to the main-sequence lifetime for stars in this mass range, it implied that the λ Bootis phenomenon should be restricted to the end of the main-sequence phase. Second, mixing via meridional circulation was not included in the computations of MC86. This appeared as a potential problem because circulation velocities decrease more slowly with depth than typical gravitational settling velocities. Since the model is based on the advection to the surface of material initially located deep in the envelope and is depleted by chemical separation throughout the first half of main-sequence evolution, any additional deep mixing may prevent the development of deep underabundances. This would make their appearance at the surface at later epochs impossible.

Since then, additional observational work has generated further potential problems for the model. Gray (1988) showed that λ Bootis stars were often found relatively close to the ZAMS. This, as discussed above, is known to be difficult to reconcile with the original diffusion-based model as put forth by MC86, and is a serious problem. Furthermore, the large underabundances (by factors of up to 100) determined by Venn & Lambert (1990) for their three λ Bootis stars appear very difficult to produce within the framework of MC86's original model. Clearly, a second look at the diffusion/mass loss model for λ Bootis stars is in order at this juncture.

This paper focuses on the second of the original two difficulties with the model of MC86, namely the impeding effect of rotationally induced meridional circulation on chemical separation. This involves carrying out particle transport calculations including the usual mechanisms leading to chemical separation—gravitational settling, differential thermal diffusion, and diffusion via differential radiative acceleration— as well as meridional circulation *and* mass loss. With the exception of the inclusion of mass loss, this has been successfully carried out in the past (e.g., Charbonneau & Michaud 1988, CM91). Accordingly, § 2 below deals mostly with the introduction of mass loss in the transport equation, in terms of both mathematical and numerical implementation. Numerical solutions for two representative elements, titanium and calcium, are presented in § 3. These show unambiguously that the original diffusion/mass loss model of MC86 no longer yields the required abundance patterns when circulation is included, as it should, in the transport calculations. Caveats and alternative theoretical models are then discussed in § 4 and a few observational tests that may help to discriminate between the various theoretical models are suggested.

2. MATHEMATICAL FORMULATION

2.1. *Transport Equation*

The formulation of the transport problem in a stellar envelope has been discussed elsewhere (see, e.g., CM91, and references therein), and so will only be briefly outlined here. Transport of a *trace* element by a total velocity field $\boldsymbol{U}$, and subject to diffusive mixing parameterized by a total diffusion coefficient D, must satisfy a conservation equation having the general form:

$$\rho \frac{\partial c}{\partial t} = -\nabla \cdot [-\rho D \nabla \ln c(\boldsymbol{x}, t) + \rho \boldsymbol{U} c(\boldsymbol{x}, t)] - \rho S_{\rm nuc}\, c(\boldsymbol{x}, t) \quad \boldsymbol{x} \in \Omega . \tag{1}$$

subject to boundary conditions which, in the absence of mass loss or accretion, can usually be brought to the form of a Neumann condition:

$$\boldsymbol{n} \cdot \nabla c(\boldsymbol{x}, t) = 0 , \quad \forall t, \boldsymbol{x} \in \partial\Omega \tag{2}$$

where $\boldsymbol{n}$ is a unit vector normal to the domain boundary $\partial\Omega$. The initial condition is usually spherically symmetric, i.e., it can be written in spherical polar coordinates as

$$c(r, \theta, 0) = c_0(r) . \tag{3}$$

The velocity field $\boldsymbol{U}$ includes contributions from meridional circulation (Tassoul & Tassoul 1982), gravitational setting, diffusion driven by differential radiative acceleration, and differential thermal diffusion (e.g., Michaud 1987). The total diffusion coefficient D includes contributions from microscopic diffusion and turbulence, if present. The nuclear reaction term $S_{\rm nuc}$ is included when dealing with elements which are destroyed by proton capture in the upper envelope (Li, Be, etc.). It is set to zero in the calculations presented below, but it is retained here for the sake of completeness. Equation (1) is a mass conservation statement; at a given position in the domain, any time variation of the mass of the element under study (left-hand-side) is due to either a nonvanishing divergence of the total flux (first terms on right-hand-side) or to local destruction by nuclear reactions (second term on right-hand-side).

In view of the symmetries inherent to the problem (i.e., symmetries in initial and boundary conditions, as well as in the velocity fields involved), the spatial solution domain which is, in general, two-dimensional (2D), can be reduced to the quarter meridional plane:

$$\Omega = \left\{(r, \theta) \in \Re^2 : R_0 \le r \le R_* , \quad 0 \le \theta \le \frac{\pi}{2}\right\} , \tag{4}$$

where R_* is the radius of the stellar surface and R_0 is the radius at which the "bottom" boundary condition is set. Note that in the absence of meridional circulation (i.e., for nonrotating stars), the problem becomes spherically symmetric and thus further reduces to one spatial dimension (1D). The partial differential equation (PDE) (1), together with equations (2)–(4), thus defines a 2D linear initial-boundary value problem.

The link with observations is provided by noting that, within the superficial convection zone, mixing time scales are short enough to ensure that abundances are independent of depth and/or latitude (Schatzman 1969). Furthermore, it has been argued that as far as mixing is concerned, convective overshoot is likely to effectively extend the convection zone up to the atmosphere, and, in the effective temperature range where they are distinct, to chemically "link" both hydrogen and helium superficial convection zones (Latour et al. 1981). This is now being confirmed by numerical simulations (Holweger & Stürenburg 1993; see also Sofia & Chan 1984). We therefore

[2] "deep" refers here to $\log [\Delta M(r)/M] \simeq -6$, where $\Delta M(r)/M$ measures the mass fraction *above* the spherical shell of radius r. At such a depth, $g > g_{\rm rad}$ for most elements, so that gravitational settling leads to the development of local underabundances. This, however, occurs on a much longer time scale that the development of abundance anomalies in the CZ.

assume that the portion of the envelope extending from the bottom of the lower CZ all the way to the surface is thoroughly mixed. Abundances in the photosphere are then identical to those in the CZ. For a given stellar model, once values for the equatorial rotational velocity and mass loss rate have been adopted, the model is completely defined.

2.2. *Inclusion of Mass Loss*

The introduction of mass loss in the diffusion model for FmAm stars was found to be necessary to quantitatively reproduce the observed abundance anomalies. It should be noted that the required mass-loss rate, of order $10^{-15}\ M_\odot\ \mathrm{yr}^{-1}$, is about one order of magnitude smaller than the observed mean solar mass-loss rate, and four to five orders of magnitude below the current upper limits determined, in A stars, from radio emission and/or asymetries in spectral line profiles (see Brown et al. 1989; Lanz & Catala 1992). At such low rates, no variations in luminosity or global structure (e.g., the mass-radius relation) are expected.

This is the mass-loss regime that we restrict ourselves to in what follows, i.e., we consider a chemically homogeneous, spherically symmetrical wind, of a magnitude such that the associated mass loss does not affect nuclear burning in the core in any significant manner over the whole main-sequence phase. The only noticeable effect on stellar structure is a perturbation of local hydrostatic equilibrium, which leads to the appearance of an outward-directed drift velocity (v_W); an expression for the drift velocity can be obtained through the requirement of mass conservation, which requires

$$\dot{M} = -4\pi\rho r^2 v_W \ . \tag{5}$$

where $\dot{M} < 0$ since we are dealing here with mass *loss*. Note that for a given mass-loss rate, the drift velocity is inversely proportional to the density. This implies that even a very weak mass loss may provide a significant contribution to particle transport in the outermost regions of the envelope. One could, in principle, introduce this drift velocity into the transport equation (1), by adding a mass-conserving (i.e., divergence-free) radial velocity field $\boldsymbol{U}_W = v_W \hat{\boldsymbol{e}}_r$ to the total advecting velocity field $\boldsymbol{U}$:

$$\rho \frac{\partial c}{\partial t} = -\nabla \cdot [-\rho D \nabla \ln c + \rho(\boldsymbol{U} + \boldsymbol{U}_W)c] + \rho S_{\mathrm{nuc}}\, c \ . \tag{6}$$

This, however is bound to lead to some numerical difficulties, in view of the aforementioned ρ^{-1} dependence of the mass-loss velocity field. Consider the solution in the CZ; by virtue of the nearly instantaneous mixing associated with convective motions, abundance profiles in the CZ are essentially flat. This implies that the second-order term dominates the right side of the transport equation. However, because of the ρ^{-1} dependence of v_W, this can only be achieved by letting $D \to \infty$. One then is in a situation where, within the CZ, two very large contributions must cancel each other exactly, a situation prone to roundoff problems. Furthermore, the upper boundary condition is no longer a simple Neumann condition, but becomes a mixed boundary condition, whose proper numerical implementation also introduces roundoff problems.

There exists, however, a simple way around these difficulties. It is grounded in the following two facts: (1) ultimately, the solution *within* the CZ is dominated by convective mixing, i.e., the abundance profile remains flat throughout the time evolution, and (2) the net effect of mass loss, within the CZ, is that of a "removal" of matter. Now, whether or not this removal occurs through the stellar surface via a stellar wind is of little importance. What matters is that the mass removal rate be equal to the prescribed mass-loss rate. Consider a trace contaminant present in the CZ and assume that abundances in the wind are identical to those in the photosphere. The contaminant's mass removal rate ($\Delta M/\Delta t$) through the stellar surface S_* due to mass loss is given by

$$\frac{\Delta M}{\Delta t} = -\int_{S_*} \rho(\boldsymbol{x}) v_W(\boldsymbol{x}) \bar{c}(t) dS \ , \tag{7}$$

where $\bar{c}(t)$ is the concentration in the CZ (independent of position). Using equation (5), one obtains immediately

$$\frac{\Delta M}{\Delta t} = \dot{M}\bar{c}(t) \ . \tag{8}$$

Consider now the following hypothesis; mass loss is "turned off" within the CZ (i.e., v_W is arbitrarily set to zero), but a sink term (S_W), corresponding to some as yet undefined process which behaves in a manner similar to nuclear burning, is introduced. The mass removal rate due to this "artificial" process can be written as

$$\frac{\Delta M}{\Delta t} = \int_{\mathrm{CZ}} \rho(\boldsymbol{x}) S_W\, c(\boldsymbol{x}, t) dV \ . \tag{9}$$

Now, recall that the concentration assumes, at a given time, the same value $\bar{c}(t)$ anywhere within the CZ. Furthermore, one can certainly assume, without any loss in generality, that S_W is also independent of position within the CZ. Therefore,

$$\frac{\Delta M}{\Delta t} = S_W \bar{c}(t) \int_{\mathrm{CZ}} \rho(\boldsymbol{x}) dV \ . \tag{10}$$

Note that the integral on the right-hand-side of this equation is simply the mass of the convection zone (M_{CZ}). For our "undefined" process to lead to the same mass removal as mass loss through a stellar wind, one simply equates the right-hand-side of equations (8) and (10), to obtain an expression for S_W:

$$S_W = \frac{\dot{M}}{M_{\mathrm{CZ}}} \ . \tag{11}$$

It is thus possible to replace, within the CZ *and* at its upper boundary—the stellar surface—the advecting field $\boldsymbol{U}_W$ by a sink term given by the above expression. The transport problem in the presence of mass loss now amounts to solving

$$\rho \frac{\partial c(\boldsymbol{x}, t)}{\partial t} = -\nabla \cdot [-\rho D \nabla \ln c(\boldsymbol{x}, t) + \rho(\boldsymbol{U} + \boldsymbol{U}_W)c(\boldsymbol{x}, t)] + \rho(S_{\mathrm{nuc}} + S_W)c(\boldsymbol{x}, t) \ , \tag{12}$$

with the usual initial and boundary conditions [eqs. (2) and (3) herein], and with $\boldsymbol{U}_W$ and S_W given by

$$\boldsymbol{U}_W = \begin{cases} v_W \hat{\boldsymbol{e}}_r & \text{below CZ} \ , \\ 0 & \text{within CZ} \ ; \end{cases} \tag{13}$$

$$S_W = \begin{cases} 0 & \text{below CZ} \ , \\ \dot{M}/M_{\mathrm{CZ}} & \text{within CZ} \ . \end{cases} \tag{14}$$

Using this approach eliminates the numerical problems mentioned previously; a Neumann boundary condition can be enforced at the stellar surface, and with the possible exception

of stars having a very thin CZ, the ρ^{-1} dependence in v_W is no longer problematic. The numerical technique used previously to tackle problems without mass loss can thus be used without further modifications.

2.3. *Numerical Implementation*

For computational reasons, it is preferable not to use standard spherical polar coordinates in seeking solutions to equation (12). This because very high resolution is required near the stellar surface, where many of the physical quantities relevant to the problem show extremely large—and not always monotonic—variations with depth. To use r as an independent variable while trying to maintain adequate resolution in the upper envelope then yields a highly irregular mesh. This is an undesirable state of affairs, from the numerical standpoint. Consequently, the following independent variables are used, for the "radial" and "angular" directions:

$$w(r) = \frac{\log\,[\Delta M(R_0)/M] - \log\,[\Delta M(r)/M]}{\log\,[\Delta M(R_0)/M] - \log\,[\Delta M(R_*)/M]}\,, \quad (15a)$$

$$\zeta(\theta) = 1 - \cos\,(\theta)\,, \quad (15b)$$

where $\Delta M(r)/M$ is the mass fraction located *above* the spherical shell of radius r. The use of the "angular" variable ζ increases the resolution near the equatorial plane, and further leads to the disappearance of explicit angular dependence in the mass and sink terms of the transport equation (i.e., the terms proportional to $\partial c/\partial t$ and c, respectively). The variable changes defined by equations (15a) and (15b) also map the solution domain $\Omega(r, \theta)$ to a unit square in $[w, \zeta]$, i.e., one has

$$\Omega(w, \zeta) = \{(w, \zeta) \in \Re^2 : 0 \le w \le 1,\ 0 \le \zeta \le 1\}\,, \quad (16)$$

Note finally that since the transformations for the angular and radial variables are decoupled, the corresponding Jacobian matrix remains diagonal, implying that no cross-derivatives appear in the transport equation in $[w, \zeta]$. With these choices of spatial variables, it assumes the general form

$$\mu(w)\frac{\partial c(w,\zeta,t)}{\partial t} = \frac{\partial}{\partial w}\left[\alpha_1(w)\frac{\partial c(w,\zeta,t)}{\partial w}\right] + \frac{\partial}{\partial \zeta}\left[\alpha_2(w,\zeta)\frac{\partial c(w,\zeta,t)}{\partial \zeta}\right] + \gamma_1(w,\zeta)\frac{\partial c(w,\zeta,t)}{\partial w} + \gamma_2(w,\zeta)\frac{\partial c(w,\zeta,t)}{\partial \zeta} + \beta(w)c(w,\zeta,t)\,, \quad (17)$$

where the coefficients μ, α_1, etc. contain information pertaining to the velocity fields and stellar structure (see eqs. [9]–[17] in CM91). Introducing mass loss affects only the coefficients γ_1 and β, that are now given by the following expressions:

$$\gamma_1(w, \zeta) = -A_3\,\rho r^2 (V_r + U_r + v_W)\,, \quad (18a)$$

$$\beta(w) = -10^{A_1 - A_2 w}\frac{2V_r}{r} - A_3 r^2 \frac{d(\rho V_r)}{dw} - A_3 S_W\,, \quad (18b)$$

where v_W and S_W are defined by equations (5) and (14) herein. Expressions for the velocity fields (V_r, U_r, ...) and constants (A_1, A_2, ...) can be found in CM91 and are not reproduced here.

3. RESULTS

Transport calculations are carried out in a *static* stellar envelope model having $\log\,(g) = 4.3$, $T_{\rm eff} = 8000$ K, and solar abundances. Radiative accelerations and diffusion coefficients are the same as those used in CM91. Quasi-instantaneous mixing from the base of the He CZ all the way to the surface is enforced by letting $D = 10^{10}$ cm^2 s^{-1} in that region. In the radiative part of the envelope, the only process contributing to D is ordinary microscopic diffusion. The envelope is assumed chemically homogeneous at $t = 0$, i.e., $c(w, \zeta, 0) = c_0$. An equatorial rotational velocity $v_e = 50$ km s^{-1} is adopted, corresponding to the apparent lower end of the $v \sin i$ distribution for λ Bootis stars. The meridional circulation velocity fields are computed using the formalism of Tassoul & Tassoul (1982). Following MC86, mass loss at a rate in the range 5×10^{-14}–2×10^{-13} $M_\odot$ yr^{-1} is assumed to take place, with chemical abundances in the wind identical to those in the surface layers.

We track the abundance evolution for two representative elements, titanium and calcium, over a time interval of 10^9 yr. For the 2D solutions, the governing PDE (eq. [12]) is solved on a 500×100 spatial mesh constructed from an orthogonal grid in $[w, \zeta]$. The reference 1D solutions presented in § 3.1 below are computed on a mesh made up of 1000 1D quadratic elements. In both cases the mass range covered by the variable w is $10^{-11} \le \Delta M/M \le 10^{-3}$. The time integration typically makes use of 2000 time steps. The finite element-based numerical scheme described in § 2 of CM91 is used, with the only difference that a standard Galerkin formulation is adopted here, instead of the original upwind Petrov-Galerkin formulation of CM91. This greatly reduces the risk of having the solutions polluted by spurrious numerical dissipation. Solution accuracy is monitored by conservation tests, as described in CM91 (§ 2.3).

3.1. *Solutions without Meridional Circulation*

Before examining the effects of meridional circulation, it is useful to recall briefly a few specific aspects of the abundance evolution in the original diffusion/mass loss model for λ Bootis stars, as developed by MC86 (see also Charbonneau 1992, § 3).

Figure 1 shows internal abundance profiles for titanium and calcium, in a nonrotating 8000 K main-sequence model. Gravitational settling, differential radiative acceleration, differential thermal diffusion, and ordinary microscopic diffusion are included in the calculations. Figure 1*a* and 1*b* correspond to solutions without mass loss, while Figure 1*c* and 1*d* show solutions with mass loss, at a rate of $\dot{M} = 5 \times 10^{-14}$ $M_\odot$ yr^{-1}. Figure 2 shows the corresponding curves for the time evolution of surface abundances. The surface abundance evolution for mass loss rates of $\dot{M} = 10^{-13}$ and 2×10^{-13} $M_\odot$ yr^{-1} are also shown.

Consider first titanium without mass loss (Fig. 1*a* and dotted line on Fig. 2*a*). It is almost (but not quite) supported at the base of the CZ in the envelope model used here, so that underabundances develop in the CZ. However, a region of large overabundance develops immediately below the base of the CZ (above the depth $\log\,[\Delta M/M] \simeq -8$, see Fig. 1*a*). At greater depths, underabundances again develop. This is due to both gravitational settling toward deeper layers and "pumping" of Ti into the aforementioned overabundance peak at $\log\,[\Delta M/M] \simeq -8$, and occurs on a much longer time scale than in the CZ.

The situation changes drastically when mass loss is intro-

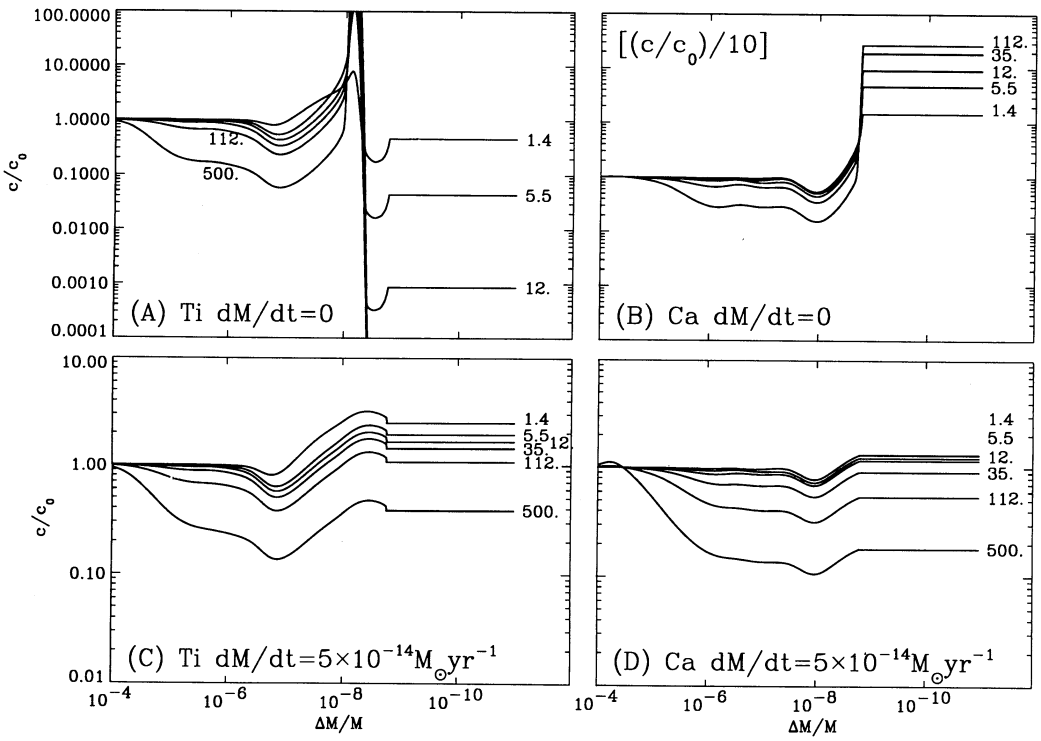

FIG. 1.—Internal concentration profiles of Ti (*panels a and c*) and Ca (*panels b and d*) in models with (*panels c and d*) and without (*panels a and b*) mass loss. Gravitational settling, differential thermal diffusion, microscopic diffusion, and differential radiative acceleration are also taken into account. All solutions are computed in a nonrotating 8000 K main-sequence model (log $g = 4.3$). The surface is to the right, and the base of the CZ is located at log $(\Delta M/M) \simeq -8.7$. Each profile is labeled according to elapsed time, in megayears. Note the change in vertical scale between panels *a* and *b*, and *c* and *d*.

duced (Fig. 1*c* and solid line on Fig. 2*a*). The abundance evolution deep in the envelope is not greatly affected. This is because mass-loss velocities decrease more rapidly ($\propto 1/\rho$) than settling velocities ($\propto T^{3/2}/Z^2\rho$) as one moves deeper in the envelope. It is higher up in the envelope, closer to the CZ, that the effects of mass loss are more strongly felt. There is no longer an overabundance peak developing above log $[\Delta M/M] \simeq -8$. This is because locally, Ti is advected upward faster than it can accumulate. As a consequence, mild *over*abundances materialize in the CZ (between 10^6 and a few 10^7 yr). This does not last long, however, since mass loss also drains the CZ from above. At later epochs, the whole upper part of the envelope has been drained of its Ti content, so that mass loss then advects in the CZ material *depleted* in Ti. At that point, underabundances materialize in the CZ (see $t = 500$ Myr curve on Fig. 1*c*). This behavior is qualitatively similar for other mass-loss rates in the range considered here.

Calcium, in a model without mass loss (Fig. 1*b* and dotted line on Fig. 2*b*), becomes overabundant in the CZ, as the net acceleration g–g_{rad} is upwardly directed at its base. A region of

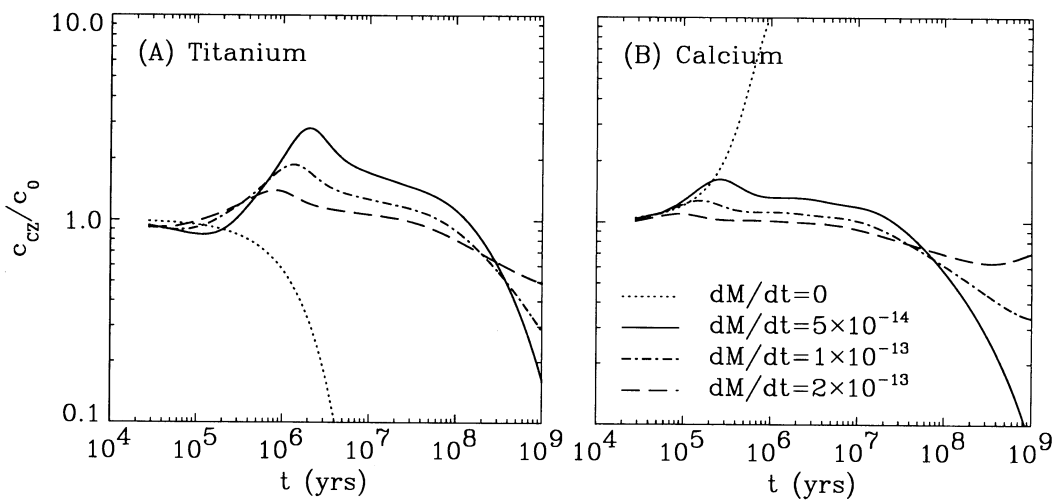

FIG. 2.—Surface abundance evolution for Ti (*panel a*) and Ca (*panel b*) in a nonrotating model undergoing mass loss. The various curves correspond to different mass-loss rates (in $M_\odot$ yr^{-1}), as indicated. Observe how significant underabundances (by a factor of 2 or more, say), require a few 10^8 yr to materialize.

underabundance develops from the base CZ down to log $[\Delta M/M] \simeq -6$. As in the case of Ti, this is due to both the upward flux into the CZ and gravitational settling operating deeper down. When mass loss is introduced (Fig. 1*d*), the outward flux at the top of the CZ greatly reduces the CZ overabundances at early epochs. The Ca-depleted material located initially deep in the envelope is eventually advected into the CZ, leading to the appearance of underabundances later on (Fig. 2*d*). Note how the levels of underabundances for Ti and Ca at late epochs are rather similar, even though the abundance evolution (in the CZ and deeper down) is markedly different at earlier epochs. Note also how generalized surface underabundances always require at least 10^8 yr to materialize.

These solutions are essentially the same as those of MC86. This is not a trivial point; although the input physics is essentially the same, the numerical solution scheme used here is completely different from that used by Michaud & Charland (see their § 3). The good agreement between the two sets of results is another indication that both of these numerical schemes succeed in catching the essence of the transport problem (compare the Ca curve at $\dot{M} = 10^{-13}\ M_\odot\ \mathrm{yr}^{-1}$ herein to the corresponding curve on Fig. 2*a* in MC86).

3.2. *Solutions with Meridional Circulation*

The appearance of generalized surface underabundances at later epochs depends on the development of underabundances deep down in the envelope throughout the earlier phases of evolution. This is the essence of the diffusion model of MC86, and it is precisely at this level that meridional circulation is likely to have significant consequences. This is because circulation velocities decrease more slowly than gravitational settling velocities as one moves deeper into the envelope. In the Tassoul & Tassoul (1982) meridional circulation solution, the magnitude of the vertical component of the circulation velocity is nearly independent of depth above log $[\Delta M/M] \sim -2$, except within a thin boundary layer located immediately below the surface. Gravitational settling velocities, on the other hand, vary roughly as $T^{3/2}/Z^2\rho$, while the drift velocity associated with mass loss varies as $1/\rho$. Both of these then decrease with increasing depth. This means that meridional circulation is likely to be the dominating transport process deep down in the envelope, even though it may be less important at the base of the CZ.

Figure 3 (Plate 19) shows snapshots (in $[w, \zeta]$) at $t = 500$ Myr of internal abundance distributions of Ti (left column) and Ca (right column), in a nonrotating model having $\dot{M} = 5 \times 10^{-14}\ M_\odot\ \mathrm{yr}^{-1}$ (top row), and rotating models having $\dot{M} = 5 \times 10^{-14}\ M_\odot\ \mathrm{yr}^{-1}$ (middle row), $\dot{M} = 2 \times 10^{-13}\ M_\odot\ \mathrm{yr}^{-1}$ (bottom row). Element concentration is now color-coded on a logarithmic scale covering the interval $0.1 \leq c/c_0 \leq 5$. Within this scheme, regions of underabundance show up in dark green, whereas regions of overabundances show up in pink. Recall that, in view of equations (15), $\zeta = 0$ correspond to the polar axis, $\zeta = 1$ to the equatorial plane, and $w = 1$ the surface. The base of the CZ is indicated by a dotted line.

The nonrotating models show spherically symmetric (i.e., ζ-independent) abundance distributions. These are the color-coded versions of the $t = 500$ Myr profiles on Figures 1*c*–1*d*. The underabundance region located deep in the envelope is clearly apparent, for both Ca and Ti (green, in the interval $0.2 \lesssim w \lesssim 0.6$). It has actually begun to penetrate into the CZ, in which moderate underabundances have already materialized. Turning to the rotating models, it is immediately obvious that circulation, even for $v_e = 50$ km s^{-1}, has had a drastic influence on the internal abundance distributions. The regions of large underabundances seen in the nonrotating solutions are almost completely absent in the rotating models. As a consequence, there are no underabundances to be advected upward at later epochs, and surface underabundances never materialize. This shows-up quite clearly on the surface abundance evolution curves, as illustrated on Figure 4. While nonrotating models develop underabundances beyond a few 10^8 yr, rotating models never do so.

Similar results are obtained for Sc and Mn, as well as in 7500 K envelope models and/or at higher rotation rates. Meridional circulation has a determining influence within the diffusion/mass-loss model for λ Bootis stars.

4. DISCUSSION

The results described above certainly raise serious doubts as to the validity of the diffusion/mass-loss model for λ Bootis

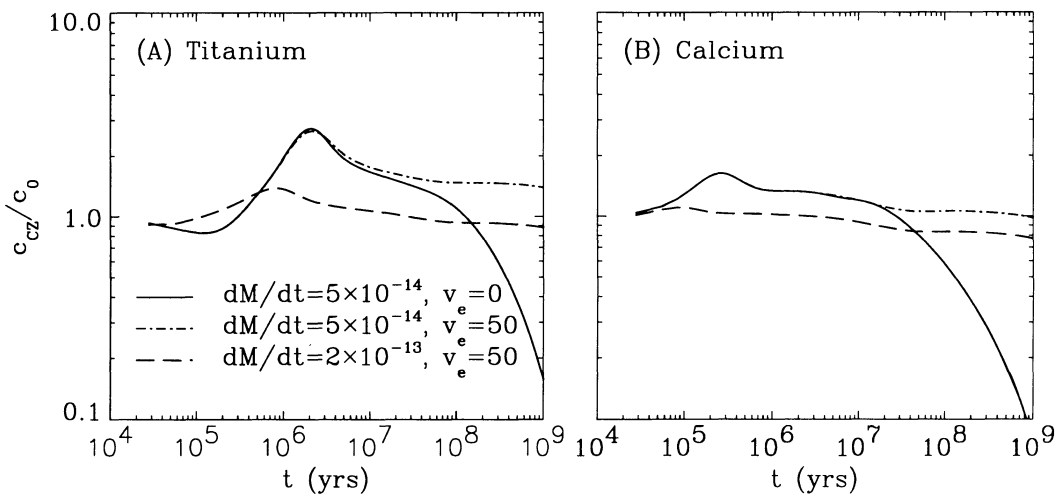

FIG. 4.—Surface abundance evolution for Ti (*panel a*) and Ca (*panel b*) in a 8000 K main-sequence model rotating with $v_e = 50$ km s^{-1}, for various mass loss rates (in $M_\odot$ yr^{-1}, as indicated). The solid lines correspond to a nonrotating model, and are shown for comparison. Notice how significant underabundances no longer materialize, at any epoch of the evolution.

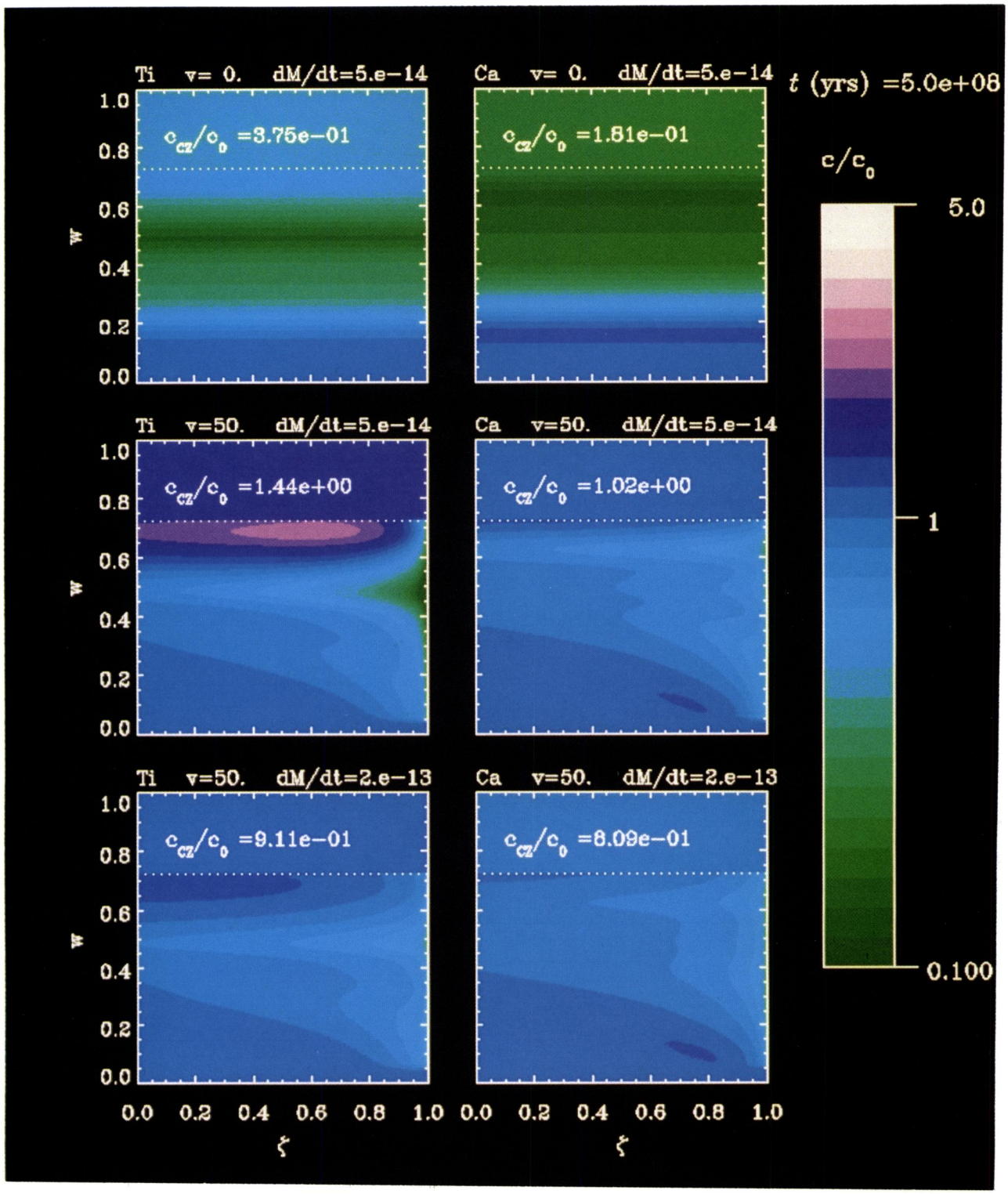

FIG. 3.—Snapshots in the $[w, \zeta]$ plane of the internal abundance distribution of Ti (*left column*) and Ca (*right column*) in a 8000 K main-sequence model undergoing mass loss. The color scale codes log (c/c_0), where c_0 is the initial ($t = 0$ concentration. The (radial) variable w covers the range $-3 \leq \log [\Delta M(r)/M] \leq -11$, and the (horizontal) dotted line indicates the base of the CZ. Efficient mixing due to convection is assumed to keep CZ chemically homogeneous. The polar axis correspond to the $\zeta = 0$ segment, and the equatorial plane to $\zeta = 1$. Including meridional circulation in the transport equation has a drastic effect on the internal abundance distributions (see text).

CHARBONNEAU (see 405, 725)

stars, yet some care is required in drawing conclusions. The above computations were carried out in a static envelope model, even though 10^9 yr represents a substantial fraction of the main-sequence lifetime for stars in this mass range. The radius of a 2 $M_\odot$ star increases by nearly a factor of 2 between its arrival on the ZAMS and the end of its main-sequence phase. The associated change in moment of inertia will lead to a reduction of the rotation rate, and in turn of the efficiency of meridional circulation mixing. The decrease in $T_{\rm eff}$ accompanying the evolution on the main-sequence also leads to a deepening of the outer CZ, and chemical separation in the outer envelope is likely to be significantly affected by changes in luminosity and by variations in the outer temperature and density profile. The surface gravity also decreases from $\log(g) \simeq 4.4$ down to $\log(g) \simeq 3.8$, leading to a corresponding decrease in the efficiency of gravitational settling. How the combination of these various effects alters the abundance evolution is difficult to predict a priori, warranting further computations along these lines.

One may also argue that the strong influence of meridional circulation demonstrated above may well be dependent on the specific circulation model adopted herein. In particular, one may argue that strong horizontal turbulence is present in the radiative interior. As this is known to reduce the efficiency of advective transport by circulation (CM91, § 5.2; Chaboyer & Zahn 1992), it represents a way to salvage the original diffusion/mass-loss model of MC86. While this cannot be strictly ruled out, it constitutes a rather ad hoc position. Furthermore, one then faces the problem of making such circulation/turbulence model compatible not only with the diffusion/mass-loss model of MC86 for λ Bootis stars, but also with the constraints posed by the (very successful) diffusion models for FmAm and HgMn stars.

There is, however, new observational evidence that is clearly incompatible with the diffusion/mass-loss model for λ Bootis stars. Gray & Corbally (1993) have unambiguously identified a very young λ Bootis star in the Orion OB1 association. As the star's membership in the association appears well established, this provides a definite counterexample to the predictions of the original diffusion/mass-loss model. Taken together with the results discussed above, this indicates that the diffusion/mass-loss model for λ Bootis stars, at least in the form originally developed by MC86, is to be abandoned.

It then becomes relevant at this juncture to investigate other mechanisms that could lead to abundance signatures characteristic of the λ Bootis phenomenon. One such mechanism is the accretion of metal-depleted material. This was originally suggested by Venn & Lambert (1990), upon noting that the abundance anomalies that they deduced from their spectroscopic work bear some striking similarities to those observed in circumstellar gas depleted in metals by grain formation. Following this lead, Charbonneau (1991) showed, using a simple diffusion/accretion model, that many of the properties of λ Bootis stars would be reproduced in such an accretion scenario. In particular, the restriction to the relatively narrow spectral type interval F0–A0 can be reproduced naturally within the framework of such a model, providing that accretion occurs at a rate of order $10^{-13}\ M_\odot\ {\rm yr}^{-1}$. Difficulties still exist; obtaining the desired level of underabundances appears to require a rather delicately tuned accretion rate. Furthermore, the assumption of gas accretion occurring without grain accretion is rather ad hoc, and may even be considered unrealistic in the light of recent computations of grain formation in winds (MacGregor & Stencel 1992). Yet the preliminary results of Charbonneau (1991) are encouraging, and certainly justify carrying out detailed, self-consistent calculations of chemical separation in the presence of accretion and meridional circulation. Such work is under way and will be presented in a forthcoming paper (Turcotte & Charbonneau 1993).

Observationally, support for the accretion-based explanation for λ Bootis stars can be sought by trying to detect unambiguous evidence of accretion around these objects. A number of λ Bootis show an infrared excess (Sadakane & Nishida 1986; see also King & Patten 1992), and a few exhibit absorption in the core of their Ca II K and/or Na D lines (Gray 1988; Holweger & Stürenburg 1991). Demonstrating that *all* λ Bootis stars show some evidence of accretion or the presence of circumstellar gas and/or grains would profide additional support for this alternative model.

I wish to thank K. B. MacGregor and G. Michaud for their critical reading of the first draft of this paper. Computations reported here were carried out on the Cray Y-MP/864 of the National Center for Atmospheric Research.

REFERENCES

Baschek, B., & Searle, L. 1969, ApJ, 155, 537
Baschek, B., & Slettebak, A. 1988, A&A, 207, 112
Bohlender, D. A., & Landstreet, J. D. 1990, MNRAS, 247, 606
Brown, A., Vealé, A., Judge, P., Bookbinder, J. A., & Hubeny, I. 1990, ApJ, 361, 220
Cayrel, R., Burkhart, C., & Van't Veer, C. 1991, in IAU Symp. 145, Evolution of Stars: The photospheric Abundance Connection, ed. G. Michaud & A. Tutukov (Dordrecht: Kluwer), 99
Chaboyer, B., & Zahn, J.-P. 1992, A&A, 253, 173
Charbonneau, P. 1991, ApJ, 372, L33
———. 1992, JRASC, 86, 31
Charbonneau, P., & Michaud, G. 1988, ApJ, 327, 809
———. 1991, ApJ, 370, 693 (CM91)
Gerbaldi, M., & Faraggiana, R. 1993, in IAU Colloq. 138, Peculiar versus Normal Phenomena in A-Type and Related Stars, ed. M. M. Dworetski, F. Castelli, & R. Faraggiana, in press
Gray, R. O. 1988, AJ, 95, 220
Gray, R. O., & Corbally, C. J. 1993, in IAU Colloq. 138, Peculiar versus Normal Phenomena in A-Type and Related Stars, ed. M. M. Dworetski, F. Castelli, & R. Faraggiana, in press
Holweger, H., & Stürenburg, S. 1991, A&A, 252, 255
Holweger, H., & Stürenburg, S. 1993, in IAU Colloq. 138, Peculiar versus Normal Phenomena in A-Type and Related Stars, ed. M. M. Dworetski, F. Castelli, & R. Faraggiana, in press
King, J. R., & Patten, B. M. 1992, MNRAS, 256, 571
Lanz, T., & Catala, C. 1992, A&A, 257, 663
Latour, J., Toomre, J., & Zahn, J.-P. 1981, ApJ, 248, 1081
MacGregor, K. B., & Stencel, R. 1992, ApJ, 397, 644
Michaud, G. 1987, Phys. Scripta, 36, 112
Michaud, G., & Charland, Y. 1986, ApJ, 311, 326 (MC86)
Michaud, G., Tarasick, D., Charland, Y., & Pelletier, C. 1983, ApJ, 269, 239
Morgan, W. W., Keenan, P. C., & Kellman, E. 1943, An Atlas of Stellar Spectra (Univ. of Chicago Press)
Preston, G. W. 1974, ARA&A, 12, 257
Sadakane, K., & Nishida, M. 1986, PASP, 98, 685
Schatzman, E. 1969, A&A, 3, 331
Sofia, S., & Chan, K. L. 1984, ApJ, 282, 550
Tassoul, J.-L., & Tassoul, M. 1982, ApJS, 49, 317
Turcotte, S., & Charbonneau, P. 1993, ApJ, submitted
Venn, K. A., & Lambert, D. L. 1990, ApJ, 363, 234